PAPER

CrossMark
click for updates

Synthesis, characterization and photovoltaic properties of azadipyrromethene-based acceptors: effect of pyrrolic substituents†

Wasana Senevirathna, Jia-yu Liao, Zhenghao Mao, Jun Gu, Matthew Porter, Chunlai Wang, Roshan Fernando and Geneviève Sauvé*

Azadipyrromethene derivatives are conjugated molecules with high absorptivity in the visible to near-IR region and high electron affinity that have great potential as electron acceptors for solar harvesting applications. To fully take advantage of these molecules, it is necessary to understand their structure–property relationships. We recently showed that phenylethynyl pyrrolic substituents red-shifted the visible absorption band, increased the electron affinity, and significantly improved the device performance in organic photovoltaic devices. Here, we synthesized and characterized a series of azadipyrromethene derivatives and their chelates, where the pyrrolic substituents were chosen to examine the effect of ethynyl group, aryl group and alkyl solubilizing group. Using thienylethynyl or alkoxyphenylethynyl substituents caused a small red-shift of the absorption compared to phenylethynyl substituents. The zinc(II) complexes were blended with regioregular poly(3-hexylthiophene) as the electron donor and tested in organic solar cells. All fullerene-free solar cells studied showed good photovoltaic properties, with power conversion efficiencies ranging from 2% to 4%. The blend films all had similar AFM images with no evidence of large-scale segregation. When comparing solubilizing groups on the pyrrolic substituents, we find that the performance varied as follows: H > *t*-butyl > 2-ethylhexyl. These results pave the way for developing higher performance non-fullerene acceptors for organic photovoltaic devices.

Introduction

Organic photovoltaic devices (OPVs) hold great promise for providing sustainable, low cost electrical energy.[1,2] In particular, solution-processed bulk heterojunction (BHJ) OPVs can be produced on a large scale using current printing technology.[3,4] Power conversion efficiencies have climbed rapidly over the past 15 years, reaching ~10% for single layer devices.[5,6] The active layer of BHJ OPVs typically consists of a conjugated polymer (or molecule) electron donor blended with a fullerene derivative as the electron acceptor. Fullerene derivatives have been the electron acceptor of choice because they work well: fullerenes can accept several electrons reversibly, have good electron transport properties,[7] have a large spherical shape,[8,9] and can form favorable nano-scale phase separation with typical electron donor materials.[10] However, fullerenes do not significantly contribute to light harvesting at wavelengths greater than 600 nm and their energy levels cannot be easily tuned, factors that seriously limit achievable efficiencies for OPVs.[7] Recent efforts demonstrated that non-fullerene acceptors can be used to overcome some of these disadvantages.[11–23] Most successful non-fullerene organic materials include sub-phthalocyanines, rylene diimide-based molecules and polymers, as well as molecules and conjugated polymers incorporating electron-withdrawing groups such as imides, cyano, fluorine and benzothiadiazoles.[21,24–29]

One overlooked candidate for designing non-fullerene acceptors is azadipyrromethene (Fig. 1). Azadipyrromethenes are bidentate ligands with strong visible absorption, tunable properties through substitution and chelation, and high electron affinity.[30–32] Their BF_2^+ chelates have been investigated for photodynamic therapy applications,[33] as well as donors for organic solar cells and acceptors in molecular triads.[34] The BF_2^+ chelate of related dipyrromethene dyes has also been demonstrated as an acceptor in OPVs.[35] We recently demonstrated that the homoleptic zinc(II) complex of di(phenylethynyl) tetraphenylazadipyrromethene is an effective electron acceptor for organic solar cells, with a power conversion efficiency of as high as 4.1% when blended with the common donor poly(3-hexylthiophene) (P3HT).[36,37] Interestingly, the power conversion efficiency of this acceptor was three times higher than when

Department of Chemistry, Case Western Reserve University, Cleveland, Ohio 44106, USA. E-mail: genevieve.sauve@case.edu
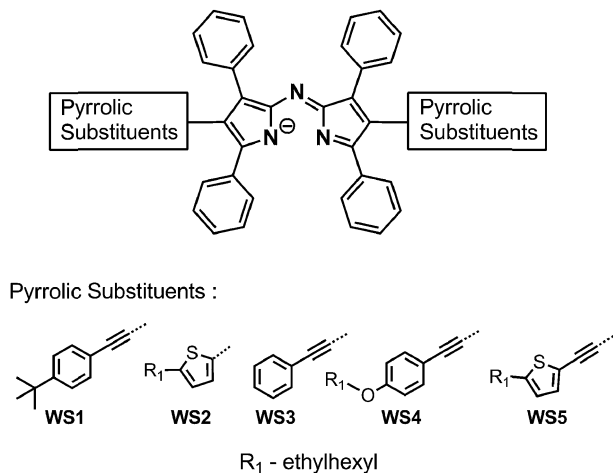
Pyrrolic Substituents :

R₁ - ethylhexyl

Fig. 1 Series of ligands with various pyrrolic substituents explored in this report.

we used a Zn(II) complex of unmodified tetraphenylazadipyrromethene as the acceptor. The better acceptor had additional phenylethynyl 'conjugated arms' at the pyrrolic positions (Fig. 1), which not only extended the conjugation system in different directions, increased electron affinity and lowered the optical energy gap, but also prevented crystallization and promoted a favorable nanoscale morphology in blends with P3HT. The idea of breaking planarity to decrease aggregation and obtain better nanoscale morphology in blends has also been reported for perylene diimides-based acceptors and other systems.[20,23,38,39] With our metal complexes, we aim to not only design nonplanar structures without impacting conjugation, but also obtain isotropic charge transport by having conjugated arms pointing in several directions.

Here, we performed a structure–property study of azadipyrromethene ligands and their complexes, focusing on the impact of the pyrrolic substituents on optical, electrochemical and photovoltaic properties. We synthesized a series of ligands (WS1–5, Fig. 1) designed to examine the effect of ethynyl, aryl and alkyl groups in the pyrrolic substituents. We introduced thiophene in the pyrrolic substituents either directly on the ADP core (WS2) or via an ethynyl spacer (WS5) to understand the effect of ethynyl spacer on the properties. Also, thiophene groups are electron rich and should contribute to tuning the energy levels and push the absorption to the near infrared region. We also compared phenylethynyl pyrrolic substituents with various alkyl substitutions at the *para*-position of the phenyl rings: no alkyl group (WS3), *t*-butyl solubilizing group (WS1) and electron rich solubilizing group 2-ethylhexyloxy (WS4). The BF₂⁺ and Zn(II) chelates for all ligands were synthesized and characterized. We found that the Zn(II) chelates all performed well as acceptors in organic photovoltaic devices, with power conversion efficiencies ranging from 2 to 4%. The best performance was obtained with the phenylethynyl pyrrolic substituents that have no solubilizing groups.

Experimental

Materials and instrumentation

Solvents and reagents were purchased from commercial suppliers, Fischer or Aldrich, and used without further purification unless indicated. Azadipyrromethene (H(ADP)) and iodinated H(ADP) (ADPI₂) were synthesized according to published methods. ^{1}H NMR, and ^{19}F NMR spectra were recorded on a Varian AS-400 spectrometer. Chemical shifts (^{1}H) are reported in parts-per-million relative to Si(CH₃)₄. Elemental analysis (C, H, and N) was performed using the optimum combustion conditions by Robertson Microlit Laboratories. UV-Vis spectra were collected on a Cary 500 spectrophotometer in HPLC grade chloroform or on a 1 cm wide glass plate. MALDI-TOF MS spectra were acquired in reflective negative mode on a Bruker autoflex III smartbeam MALDI-TOF TOF spectrometer. Thermal gravimetric analysis (TGA) was performed on a TA instrument Q500 thermogravimetric analyzer.

Synthesis

Tributyl(4-tert-butylphenylethynyl)tin (A1). 4-*tert*-Butylphenylacetylene (3.5 g, 22.1 mmol) was added into a 250 mL Schlenk flask. The flask was evacuated and refilled (×3) with N₂. Then 20 mL of dry diethyl ether was added and the solution was degassed for 5 min. The flask was cooled using a CHCl₃/dry ice bath. *n*-BuLi (8.85 mL, 22.1 mmol) was added dropwise *via* a syringe. After ~10–15 min, the cold bath was removed and the reaction mixture was allowed to reach room temperature. The solution became pale brown. After 30 min, the reaction mixture was cooled using an acetonitrile/dry ice bath. Bu₃SnCl (6.0 mL, 22.1 mmol) was added dropwise *via* a syringe. After ~10 min, the cold bath was removed and the reaction mixture was allowed to reach room temperature. Upon warming, a white suspension was formed. After stirring at room temperature for ~1 h, the mixture was dried by rotary evaporation. The oily residue was dissolved in hexanes and vacuum filtered. The filtrate was taken and the solvent was removed by vacuum evaporation. A yellow oil was obtained (A1). Yield: 9.6 g, 98%. ^{1}H NMR (400 MHz, CDCl₃, δ): 7.36–7.38 (m, 2H), 7.27–7.29 (m, 2H), 1.55–1.65 (m, 6H), 1.28 (s, 9H), 1.32–1.40 (m, 6H), 1.01–1.05 (t, J = 8 Hz, 6H), 0.86–0.92 (t, J = 4 Hz, 9H).

(5-(2-ethylhexyl-2-thiophene)trimethyl)tin (A2). This was synthesized according to a literature procedure.[40] A pale yellow oil was obtained (A2). Yield: 5.04 g. 71%. ^{1}H NMR (400 MHz, CDCl₃, δ): 6.82–6.84 (d, J = 8 Hz, 1H), 6.49–6.50 (d, J = 4 Hz, 1H), 2.63–2.67 (t, J = 8 Hz, 2H), 1.50 (m, 1H), 1.21–1.32 (m, 8H), 0.80–0.89 (m, 9H).

Tributyl(phenylethynyl)tin (A3). The same procedure was used as that for A1, using ethynylbenzene. A yellow oil was obtained (A3). Yield: 18.5 g, 97%. ^{1}H NMR (400 MHz, CDCl₃, δ): 7.43–7.46 (m, 2H), 7.25–7.28 (m, 3H), 1.55–1.64 (m, 6H), 1.33–1.42 (m, 6H), 1.04–1.08 (t, J = 8 Hz, 6H), 0.91–0.94 (t, J = 4 Hz, 9H).

Tributyl(4-(2-ethylhexyloxy)phenylethynyl)tin (A4). The same procedure was used as that for A1, using 1-((2-ethylhexyl)oxy)-4-ethynylbenzene (iv) (synthesis of iv can be found in ESI†). A yellow oil was obtained (A4). Yield: 10.0 g, ~99%. ^{1}H NMR (400 MHz, CDCl₃, δ): 7.35–7.37 (m, 2H), 6.77–6.79 (m, 2H), 3.80–

3.81 (m, 2H), 1.68–1.74 (m, 1H), 1.32–1.44 (m, 10H), 1.26–1.31 (m, 4H), 1.56–1.64 (m, 6H), 1.01–1.05 (m, 6H), 0.86–0.96 (m, 15H).

Tributyl((5-(2-ethylhexyl)thiophen-2-yl)ethynyl)tin (A5). The same procedure was used as that for **A1**, using 2-(2-ethylhexyl)-5-ethynylthiophene (**vii**) (synthesis of **vii** can be found in ESI†). A yellow oil was obtained (**A5**). Yield: 8.4 g, 97%. ^{1}H NMR (400 MHz, CDCl$_3$, δ): 6.98–6.99 (d, J = 4 Hz, 1H), 6.55–6.56 (d, J = 4 Hz, 1H), 2.67–2.68 (d, J = 4 Hz, 2H), 1.54–1.57 (m, 1H), 1.30–1.37 (m, 26H), 0.85–0.92 (m, 15H).

Synthesis of free ligands, H(WS1–5)

H(WS1). Compound **A1** (0.581 g, 1.311 mmol) and ADPI$_2$ (0.307 g, 0.437 mmol) were charged into a dry 50 mL flask and put under vacuum for ~10 min. The flask was evacuated and refilled (×3) with N$_2$. Dry *m*-xylene (50 mL) was added *via* a syringe and stirred for ~5 min under inert conditions. The Pd(PPh$_3$)$_4$ (50 mg, 10% mmol) catalyst was added inside a glove box. The reaction mixture was heated to 125 °C under N$_2$ for 36–48 h. Upon heating, the solution color changed from purple to deep blue. The solvent was removed by rotary evaporation and the product was triturated with cold methanol (10 mL) and washed with cold ether (10 mL × 3), until a pale blue coloration appeared. The crude product was purified by column chromatography with silica gel and dichloromethane (DCM). Yield: 238 mg, 71%. ^{1}H NMR (400 MHz, CDCl$_3$, δ): 8.31–8.33 (d, J = 8.0 Hz, 4H), 8.16–8.19 (d, J = 8.0 Hz, 4H), 7.43–7.52 (m, 6H), 7.35–7.42 (m, 14H), 1.31 (s, 18H). MALDI-TOF MS: *m/z* calcd for C$_{56}$H$_{47}$N$_3$ 761.38, found 760.38.

H(WS2). The same procedure was used as that for H(WS1), using **A2** and ADPI$_2$. Yield: 262 mg, 88%. ^{1}H NMR (400 MHz, CDCl$_3$, δ): 7.53–7.58 (m, 8H), 7.32–7.37 (m, 6H), 7.20–7.21 (m, 6H), 6.64 (s, 4H), 2.69–2.71 (d, J = 8.0 Hz, 4H), 1.50 (m, 2H), 1.25–1.32 (m, 16H), 0.84–0.87 (m, 12H). MALDI-TOF MS: *m/z* calcd for C$_{56}$H$_{59}$N$_3$S$_2$ 837.42, found 836.39. Elem. anal. calcd: C, 80.24; H, 7.09; N, 5.01; S, 7.65, found: C, 80.03; H, 7.18; N, 4.88; S, 7.44.

H(WS3). The same procedure was used as that for H(WS1), using **A3** and ADPI$_2$. Yield: 135 mg, 28%. ^{1}H NMR was not available due to poor solubility. MALDI-TOF MS: *m/z* calcd for C$_{48}$H$_{31}$N$_3$ 649.25, found 648.18. Elem. anal. calcd: C, 88.72; H, 4.81; N, 6.47, found: C, 87.80; H, 5.19; N, 6.23.

H(WS4). The same procedure was used as that for H(WS1), using **A4** and ADPI$_2$. Yield: 340 mg, 66%. ^{1}H NMR (400 MHz, CDCl$_3$, δ): 8.30–8.32 (d, J = 8 Hz, 4H), 8.18–8.20 (d, J = 8 Hz, 4H), 7.50–7.56 (m, 6H), 7.37–7.40 (m, 12H), 6.86–6.88 (d, J = 8.0 Hz, 4H), 3.83–3.85 (dd, J = 8.0 Hz 4H), 1.72 (m, 2H), 1.43–1.50 (m, 8H), 1.30–1.32 (m, 8H), 0.88–0.92 (m, 9H). MALDI-TOF MS: *m/z* calcd for C$_{64}$H$_{63}$N$_3$O$_2$ 905.49, found 904.32. Elem. anal. calcd: C, 84.82; H, 7.01; N, 4.64, found: C, 84.78; H, 6.86; N, 4.61.

H(WS5). The same procedure was used as that for H(WS1), using **A5** and ADPI$_2$. Yield: 173 mg, 65%.^{1}H NMR (400 MHz, CDCl$_3$, δ): 8.25–8.29 (d, J = 8 Hz, 4H), 8.15–8.17 (d, J = 8 and 4 Hz, 4H), 7.49–7.58 (m, 6H), 7.35–7.47 (m, 6H), 7.06–7.07 (d, J = 4.0 Hz, 2H), 6.67–6.68 (d, J = 4.0 Hz, 2H), 2.69–2.71 (d, J = 8.0 Hz, 4H), 1.47–1.65 (m, 2H), 1.18–1.42 (m, 16H), 0.74–0.99 (m, 12H). MALDI-TOF MS: *m/z* calcd for C$_{60}$H$_{59}$N$_3$S$_2$. 885.42, found 884.30. Elem. anal. calcd: C, 81.31; H, 6.71; N, 4.74, found: C, 81.11; H, 7.00; N, 4.71.

Synthesis of BF$_2$$^+$ chelates, BF$_2$(WS1–5)

BF$_2$(WS1) was synthesized using the literature procedure.[37]

BF$_2$(WS2). The same procedure was used as for BF$_2$(WS1), using H(WS2). Yield: 88 mg, 83%. ^{1}H NMR (400 MHz, CDCl$_3$, δ) 7.55–7.59 (d, J = 8 Hz, 4H), 7.50–7.52 (d, J = 8 Hz, 4H), 7.25–7.34 (m, 12H), 6.48–6.49 (d, J = 4 Hz, 2H), 6.40–6.41 (d, J = 4 Hz, 2H), 2.59–2.61 (d, J = 8 Hz, 4H), 1.38–1.44 (m, 2H), 1.17–1.25 (m, 16H), 0.77–0.86 (m, 12H). ^{19}F NMR (400 MHz, CDCl$_3$, δ) 132.5–132.8 (q). MALDI-TOF MS: *m/z* calcd for C$_{56}$H$_{58}$BF$_2$N$_3$S$_2$ 886.02, found 884.46. Elem. anal. calcd: C, 75.91; H, 6.60; N, 4.74; found: C, 76.11; H, 6.89; N, 4.53.

BF$_2$(WS3). The same procedure was used as for BF$_2$(WS1), using H(WS3). Yield: 63 mg, 49%. ^{1}H NMR (400 MHz, CDCl$_3$, δ): 8.24–8.27 (d, J = 8 Hz, 4H), 8.02–8.04 (d, J = 8 Hz, 4H), 7.49–7.53 (m, 12H), 7.29–7.30 (m, 10H). MALDI-TOF MS: *m/z* calcd for C$_{48}$H$_{30}$BF$_2$N$_3$ 697.25, found 696.23. Elem. anal. calcd: C, 82.6 4; H, 4.33; N, 6.02, found: C, 82.38; H, 4.61; N, 5.92.

BF$_2$(WS4). The same procedure was used as for BF$_2$(WS1), using H(WS4). Yield: 86 mg, 68%. ^{1}H NMR (400 MHz, CDCl$_3$, δ): 8.22–8.24 (d, J = 8 Hz, 4H), 7.98–8.00 (d, J = 8 Hz, 4H), 7.42–7.47 (m, 12H), 7.18–7.20 (d, J = 8 Hz, 4H), 6.76–6.78 (d, J = 8 Hz, 4H), 3.77–3.79 (d, J = 8 Hz, 4H), 1.67 (m, 2H), 1.35–1.40 (m, 8H), 1.25–1.27 (m, 8H), 0.83–0.89 (m, 12H). ^{19}F NMR (400 MHz, CDCl$_3$, δ): 131.6–131.8 (q). MALDI-TOF MS: *m/z* calcd for C$_{64}$H$_{62}$BF$_2$N$_3$O$_2$ 953.49, found 952.22. Elem. anal. calcd: C, 80.57; H, 6.55; N, 4.40, found: C, 80.34; H, 6.55; N, 4.33.

BF$_2$(WS5). The same procedure was used as for BF$_2$(WS1), using H(WS5). Yield: 51 mg 77%. ^{1}H NMR (400 MHz, CDCl$_3$, δ): 8.20–8.22 (d, J = 8 Hz, 4H), 7.98–8.00 (d, J = 8 Hz, 4H), 7.42–7.49 (m, 12H), 6.92–6.93 (d, J = 4 Hz, 4H), 6.59–6.60 (d, J = 4 Hz, 4H), 2.68–2.69 (d, J = 4 Hz 4H), 1.53 (m, 2H), 1.25–1.31 (m, 16H), 0.83–0.87 (m, 12H). ^{19}F NMR (400 MHz, CDCl$_3$, δ): 131.4–131.7 (q). MALDI-TOF MS: *m/z* calcd for C$_{60}$H$_{58}$BF$_2$N$_3$S$_2$ 933.41, found 932.22. Elem. anal. calcd: C, 77.15; H, 6.26; N, 4.50, found: C, 77.29; H, 6.37; N, 4.47.

Synthesis of Zn(ɪɪ) complexes, Zn(WS1–5)$_2$

Zn(WS1)$_2$ was synthesized using the literature procedure.[37]

Zn(WS2)$_2$. The same procedure was used as for Zn(WS1)$_2$, using H(WS2). Synthesis involved the reaction between H(WS2) (0.404 g, 0.482 mmol) and zinc acetate [Zn(OAc)$_2$] (0.115 g, 0.628 mmol) reflux in 50 mL of 1-butanol at 125 °C for 2 h. The solvent was evaporated and the crude was purified by column chromatography on silica gel with 1 : 1 DCM/hexanes. The solvent was evaporated and the solid residue was dissolved in a minimum amount of DCM. The dark blue solid was isolated by slow evaporation of DCM. Yield: 83 mg, 92%. ^{1}H NMR (400 MHz, CDCl$_3$, δ): 7.31–7.33 (m, 8H), 7.18–7.20 (m, 12H), 7.00–7.13 (m, 20H), 6.51 (d, J = 4 Hz, 4H), 6.38 (d, J = 4 Hz, 4H), 2.62–2.64 (m, 8H), 1.45–1.47 (m, 4H), 1.22–1.30 (m, 32H), 0.81–0.85 (m, 24H). MALDI-TOF MS: *m/z* calcd for C$_{112}$H$_{116}$N$_6$S$_4$Zn 1737.75, found 1738.63. Elem. anal. calcd: C, 77.32; H, 6.72; N, 4.83; found: C, 77.34; H, 6.82; N, 4.75.

Zn(WS3)$_2$. The same procedure was used as for Zn(WS2)$_2$, using H(WS3). Yield: 176 mg, 54%. ^{1}H NMR (400 MHz, CDCl$_3$, δ): 7.97–7.99 (m, 8H), 7.78–7.76 (m, 8H), 7.45–7.46 (m, 12H),

7.35–7.37 (m, 8H), 7.27–7.29 (m, 12H), 7.21–7.23 (m, 12H). MALDI-TOF MS: m/z calcd for $C_{96}H_{60}N_6Zn$ 1361.42, found 1360.77. Elem. anal. calcd: C, 84.60; H, 4.44; N, 6.17, found: C, 84.42; H, 4.36; N, 6.08.

$Zn(WS4)_2$. The same procedure was used as for $Zn(WS2)_2$, using H(WS4). Yield: 123 mg, 96%. ^{1}H NMR (400 MHz, CDCl$_3$, δ): 7.98–8.00 (m, 8H), 7.75–7.77 (m, 8H), 7.43–7.45 (m, 14H), 7.26–7.28 (m, 8H), 7.19–7.21 (m, 10H), 6.80–6.82 (m, 8H), 3.81–3.82 (d, $J = 4$ Hz, 8H), 1.68–1.73 (m, 4H), 1.36–1.48 (m, 16H), 1.28–1.30 (t, $J = 4$ Hz, 16H), 0.88–0.92 (t, $J = 8$ Hz 24H). MALDI-TOF MS: $C_{128}H_{124}N_6O_4Zn$ m/z calcd 1873.90, found 1872.60. Elem. anal. calcd: C, 81.96; H, 6.66; N, 4.48, found C, 82.26; H, 6.89; N, 4.43.

$Zn(WS5)_2$. The same procedure was used as for $Zn(WS2)_2$, using H(WS5). Yield: 180 mg, 80%. ^{1}H NMR (400 MHz, CDCl$_3$, δ): 7.92–7.94 (m, 8H), 7.69–7.71 (m, 8H), 7.41–7.43 (m, 12H), 7.19–7.20 (m, 12H), 6.92–6.93 (d, $J = 4$ Hz, 4H), 6.59–6.60 (d, $J = 4$ Hz, 4H), 2.67–2.69 (d, $J = 8$ Hz, 8H), 1.51 (m, 4H), 1.26–1.31 (m, 16H), 0.84–0.88 (m, 24H). MALDI-TOF MS: $C_{120}H_{116}N_6S_4Zn$ m/z calcd 1833.75, found 1833.72. Elem. anal. calcd: C, 78.51; H, 6.37; N, 4.58, found C, 78.74; H, 6.49; N, 4.43.

Electrochemistry

Cyclic voltammetry experiments were conducted using an Auto-Lab-PGSTAT 302N, Eco Chemie potentiostat at room temperature. All glassware was thoroughly cleaned and oven-dried overnight before use. Dichloromethane (DCM) was distilled over calcium hydride and stored in a nitrogen glovebox. Ferrocene was purified by sublimation. A typical three-electrode configuration was used, with a glassy carbon electrode as the working electrode and two platinum wires as counter and pseudo-reference electrodes. Ferrocene/ferrocenium was used as an internal standard. The measurements were performed with a scan rate of 0.1 V s^{-1} in degassed DCM with tetra-n-butylammoniumhexafluorophosphate (0.1 M TBAPF$_6$) as the supporting electrolyte. The electrolyte was purged with nitrogen for ~10 min prior to each measurement.

Film characterization

Samples for the film absorption were prepared by spin coating (400 rpm for 1 min), a filtered (0.2 μm PTFE filter) solution of P3HT (10 mg mL^{-1}) for the neat P3HT film and solutions of ADP-based materials (10 mg mL^{-1}) for neat films, or solutions of 10 mg mL^{-1} of P3HT and 10 mg mL^{-1} acceptor for the 1 : 1 w/w blend films. All solutions were prepared using HPLC grade CHCl$_3$. UV-Vis spectra were collected on a Cary 500 spectrophotometer. Fluorescence emission spectra were recorded using a Cary Eclipse fluorescence spectrometer. Atomic force microscopy (AFM) measurements were performed on an Agilent Technologies 5500 instrument in tapping mode.

Solar cell fabrication

The photovoltaic properties of $Zn(WS1–5)_2$ series were studied in a device structure of ITO/ZnO/P3HT : $Zn(WS1–5)_2$/MoO$_3$/Ag (ITO = indium tin oxide, $R = 15$ Ω sq^{-1}). A blend solution P3HT : $Zn(WS1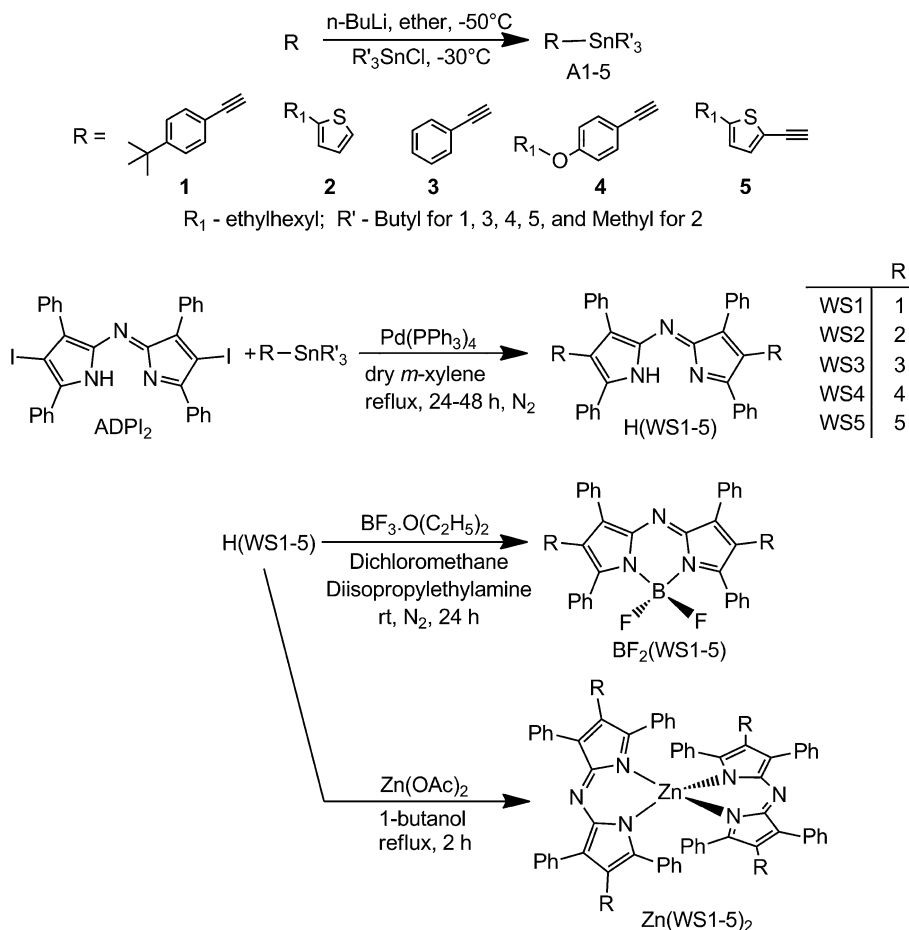–5)_2$ (w/w with a total concentration of 20 mg mL^{-1}) in o-dichlorobenzene was prepared. The ZnO layer was spin-coated on a pre-cleaned ITO substrate at 4000 rpm from a ZnO precursor solution of zinc acetate dihydrate (0.25 M) and monoethanolamine (0.25 M) in 2-methoxyethanol (solvent), and the substrate was subsequently annealed at 150 °C for 5 min. The photoactive layer of P3HT : $Zn(WS1–5)_2$ (~90 nm) was prepared by spin-coating the blend solution at 1000 rpm for 40 s and then 2000 rpm for 2 s, followed by annealing at 120 °C for 30 min. Finally, the process was completed by depositing MoO$_3$ (10 nm) and Ag (80 nm) in a sequence under a vacuum pressure of 2×10^{-6} Torr using an Angstrom Engineering Evo-vac Deposition System. The measurements of solar cells were carried out in the glove box (Pure Lab^{HE}) under 1.5 AM solar illumination at an intensity of 100 mW cm^{-2} using an Oriel Sol2A solar simulator and a Keithley 2400 IV station. The total effective area of the film was 0.17 cm^2. The IPCE was measured with a QEX10 Quantum Efficiency Measurement System.

Results and discussion

Synthesis

Azadipyrromethene dyes with various pyrrolic substituents (H(WS1–5)) were synthesized in moderate yield by Stille coupling of iodinated azadipyrromethene (ADPI$_2$) with the corresponding tributyltin derivative (Scheme 1). In our previous publication,[37] we had synthesized ligand H(WS1) using Sonogashira coupling, but purification and isolation of H(WS1) were difficult due to the presence of significant amounts of mono-substituted byproducts. Here, MALDI-TOF MS of the crude H(WS1) made by Stille coupling showed the desired product as the dominant peak, with much smaller amounts of mono-substituted byproducts than with the previous method. The higher conversion to the di-substituted product could result from a higher boiling point solvent used (m-xylene, 125 °C) than in the previous method (xylene/triethylamine, 70 °C). Furthermore, we found that washing with cold methanol and diethyl ether removed most impurities, including the mono-substituted byproduct, allowing the use of smaller columns for the final purification. These changes combined to increase the overall yield for H(WS1) from 51% using our previous method to 71% using this method. All pure ligands (H(WS1–5)) were isolated as air stable blue powders, and were characterized by ^{1}H NMR spectroscopy, MALDI-TOF MS and elemental analysis. Ligand H(WS3) could not be purified as well as the other ligands due to its limited solubility in organic solvents.

The BF$_2^+$ chelates were synthesized by reacting the free ligands H(WS1–5) with trifluoroboron etherate and diisopropylethylamine (Scheme 1). The chelates were purified by liquid–liquid extraction, followed by column chromatography with 1 : 1 DCM/hexanes to afford air-stable purple-blue powders in good yield. [19]F spectroscopy showed a quartet around ~131–132 ppm, confirming the tetracoordination state of the boron atom. Homoleptic Zn(II) complexes were synthesized by reacting H(WS1–5) with zinc acetate in 1-butanol (Scheme 1). All complexes were purified by chromatography and characterized by MALDI-TOF MS, ^{1}H NMR, and elemental analysis. MALDI-TOF MS confirmed the 1 : 2 stoichiometry ratio of metal to

Scheme 1 Synthesis of azadipyrromethene dyes with various pyrrolic substituents.

ligand for all complexes, Zn(WS1–5)$_2$. The thermal properties of ADP-based molecules were examined by thermal gravimetric analysis (Fig. S13 and Table S1 in the ESI section†). All compounds were thermally stable, with 5% weight loss onsets occurring in the range of 280–517 °C.

Electrochemistry

The electrochemical properties of the ligands and complexes were investigated by cyclic voltammetry in dichloromethane, using ferrocene/ferrocinium (Fc/Fc$^+$) as the internal reference. The electrochemical properties of all compounds are summarized in Table 1, and the cyclic voltammograms of the WS4 series are shown in Fig. 2. The cyclic voltammograms of the other compounds can be found in the ESI section.† All free ligands and BF$_2$$^+$ chelates displayed two reversible reductions and one or two irreversible oxidations, while the Zn(II) complexes exhibited two closely spaced reversible reductions and two reversible oxidations. The potential difference between the 1st $E_{1/2}$(reduction) and the 2nd $E_{1/2}$(reduction) for the free ligands (H(WS1–5)) varied from 0.55 V to 0.65. This potential difference for BF$_2$$^+$ chelates was ~0.80 V, implying that the second reduction is much harder than the first reduction. Interestingly, this potential difference is very small for Zn(II)

complexes, ~0.14 V to 0.26 V, indicating that the second reduction occurs almost as easily as the first. The ability of the Zn(II) complexes to easily accept two electrons makes them promising electron acceptors.

The effect of the pyrrolic substituents on the electrochemical properties of ADP was as expected. Phenylethynyl substituent (3) anodically (positively) shifted both the first oxidation and the first reduction potentials of the BF$_2$$^+$ chelate by 0.18 V and 0.20 V, respectively. Similarly, the first oxidation and reduction potentials of Zn(WS3)$_2$ were anodically shifted by 0.10 V and 0.17 V, respectively, relative to Zn(ADP)$_2$. The resulting energy gap is reduced due to the extended conjugation through the phenylethynyl groups. Adding electron-donating groups at the *para*-position of the phenylethynyl substituents (1, 4) further fine-tuned the electrochemical potentials by slightly shifting the potentials cathodically.

The thienyl pyrrolic substituent (2) had little effect on the first oxidation potential of the free ligand and Zn(II) complex, but cathodically shifted that of the BF$_2$$^+$ complex by 0.15 V, due to the electron-rich character of thiophene. DFT calculations indicate that conjugation is not significantly extended into the thiophene groups because they are out-of-plane relative to the ADP conjugated plane (dihedral angle between 56° and 60°).[41] Adding an ethynyl spacer between the ADP core and thiophene
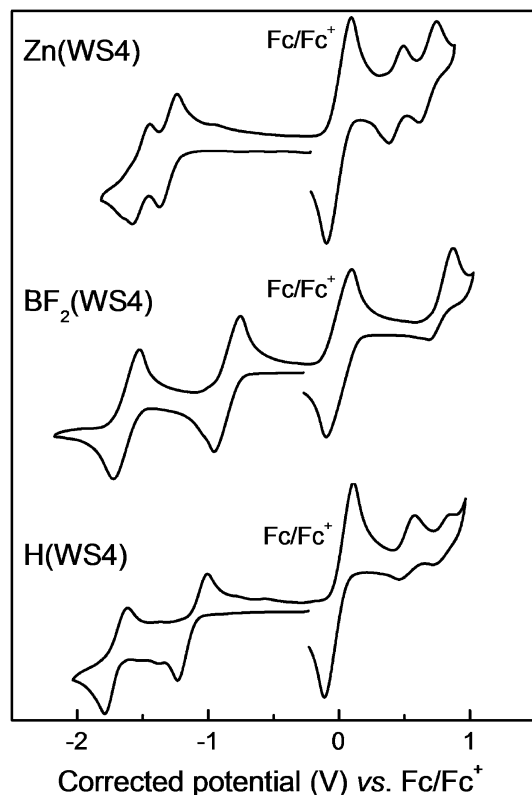
Fig. 2 Cyclic voltammograms representing H^+, BF_2^+ and Zn^{+2} chelates of WS4 in 0.1 M TBAPF dichloromethane solution and Fc/Fc^+ as the internal standard.

first oxidation potentials of the free ligands H(WS2) and H(WS5) were similar, the additional ethynyl group anodically shifted the first reduction potential of H(WS2) by 0.13 V. In the case of BF_2^+ complexes, the ethynyl group anodically shifted the oxidation and reduction potentials of BF_2(WS2) by 0.09 V and 0.15 V, respectively. A similar trend was observed for the $E_{p,a}$ and $E_{p,c}$ of the Zn(ii) complexes.

Fig. 3 summarizes the HOMO and LUMO energy levels estimated using cyclic voltammetry. The HOMO for $Zn(WS3)_2$ was −5.6 eV and the LUMO was −3.85 eV. By comparison, the LUMO estimated for PCBM in our laboratory using the same method was −3.99 eV. The HOMO and LUMO of $Zn(WS3)_2$ are lower than those of the $Zn(ADP)_2$ analogue by 0.10 eV and 0.17 eV, respectively, suggesting that the pyrrolic phenylethynyl moieties of WS3 stabilize both frontier molecular orbitals. $Zn(WS2)_2$ had higher LUMO energy levels than $Zn(ADP)_2$ due to the electron donating strength of thiophene and the fact that the thiophene is out-of-plane with ADP. Fig. 3 also includes the estimated energy levels for the common conjugated polymer donor, regioregular poly(3-hexylthiophene) (P3HT). Although the estimated energy levels are not directly comparable (film *versus* solution measurements), the lower HOMO and LUMO energy levels of the Zn(ii) complexes compared to P3HT should allow electron transfer from P3HT to the complex and hole transfer from the complex to P3HT. However, more accurate estimates of HOMO and LUMO levels are required to determine the exact energy gaps for these charge transfer processes.

Optical properties

The solution absorption spectra of the azadipyrromethene-based ligands and complexes are shown in Fig. 4 and the optical properties are summarized in Table 2. Fig. 4a compares the absorption spectra of the free ligands. They all showed a strong absorption peak in the visible range (594–633 nm) due to a

group (5) reduces the steric hindrance between thiophene hydrogens and ADP phenyl rings, thereby allowing the conjugated pyrrolic substituents to lay in the same plane as the ADP core and to extend the size of the conjugation system. While the

Table 1 Electrochemical properties in dichloromethane

	$E_{1/2}$ oxidation (V *vs.* Fc/Fc^+)	$E(p,a)$ (V *vs.* Fc/Fc^+)	$E_{1/2}$ reduction (V *vs.* Fc/Fc^+)	$E(p,c)$ (V *vs.* Fc/Fc^+)
H(ADP)	—	0.56, 0.96	−1.20, −1.85	−1.25, −1.90
BF_2(ADP)	—	0.90	−0.81, −1.61	−0.84, −1.64
$Zn(ADP)_2$	0.40, 0.69	0.46, 0.76	−1.42, −1.56	−1.48, −1.62
H(WS1)	—	0.67, 0.91	−1.05, −1.65	−1.18, −1.77
BF_2(WS1)	—	0.90	−0.71, −1.51	−0.78, −1.57
$Zn(WS1)_2$	0.47, 0.74	0.57, 0.84	−1.27, −1.48	−1.33, −1.54
H(WS2)	—	0.63, 0.95	−1.23, −1.78	−1.29, −1.86
BF_2(WS2)	—	0.75	−0.90, −1.74	−0.96, −1.80
$Zn(WS2)_2$	0.39, 0.63	0.45, 0.69	−1.51, −1.77	−1.58, −1.86
H(WS3)	[a]	—	—	—
BF_2(WS3)	—	1.08	−0.79, −1.59	−0.95, −1.75
$Zn(WS3)_2$	0.50, 0.77	0.58, 0.86	−1.25, −1.47	−1.33, −1.55
H(WS4)	—	0.58, 0.85	−1.12, −1.70	−1.23, −1.79
BF_2(WS4)	—	0.87	−0.85, −1.62	−0.95, −1.58
$Zn(WS4)_2$	0.44, 0.68	0.49, 0.74	−1.30, −1.51	−1.37, −1.75
H(WS5)	—	0.64	−1.10, −1.67	−1.18, −1.75
BF_2(WS5)	—	0.84	−0.75, −1.53	−0.81, −1.60
$Zn(WS5)_2$	—	0.52, 0.76	—	−1.27, −1.09

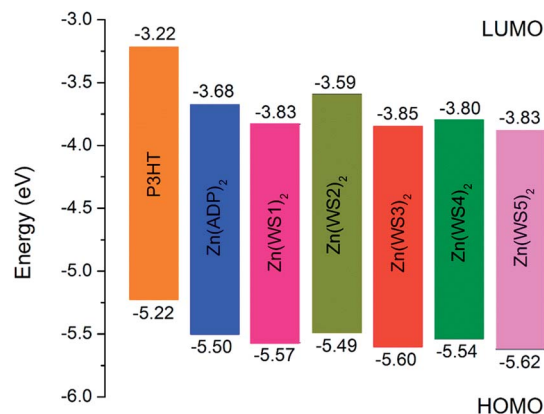[a] Could not obtain a good cyclic voltammogram of H(WS3) due to limited solubility and purity.

Fig. 3 Estimated HOMO and LUMO energy levels obtained by cyclic voltammetry from the $E_{1/2}$ values in dichloromethane solution, using the value of -5.1 eV for Fc/Fc$^+$.[42] For Zn(WS5)$_2$, $E_{p,a}$ and $E_{p,c}$ were used as an approximation to $E_{1/2}$. The HOMO and LUMO levels of P3HT films were estimated in our laboratory from the oxidation onset and the optical gap, and are included for comparison.

pyrrolic ring π–π* transition, and a strong absorption peak near 300 nm. The molar absorptivities for the visible absorption band ranged from 32×10^3 M^{-1} cm^{-1} to 47×10^3 M^{-1} cm^{-1}, where H(WS2) had the lowest and H(WS1, 4) had the highest molar absorptivity. The presence of phenylethynyl or thienylthynyl groups at pyrrolic positions lead to a bathochromic shift of $\sim$37 nm compared to the λ_{max} of H(ADP). H(WS2) has a similar absorption maximum ($\lambda_{max} = 594$ nm) than H(ADP) ($\lambda_{max} = 596$ nm), suggesting that the thiophene groups are not conjugated with the ADP core. On the other hand, when an ethynyl spacer was incorporated between the ADP core and the thiophene group, the maximum absorption red shifted by 39 nm to 633 nm for H(WS5), due to the reduced steric hindrance caused by the spacer, resulting in extended conjugation. Larger red-shifts were observed when comparing the λ_{onset}. Relative to H(ADP), the λ_{onset} for H(WS2) red-shifted by 14 nm due to the electron donating nature of thiophene, H(WS3) red-shifted by 31 nm due to extended conjugation, and H(WS1, 4, 5) red shifted by 70–90 nm, due to a combination of extended conjugation and the presence of electron donating groups in the pyrrolic substituents.

Fig. 4b compares the absorption spectra of the BF$_2$$^+$ chelates in chloroform. The absorption spectra showed a broad intense absorption peak in the near infrared region. Using thienyl pyrrolic substituents (**2**) resulted in the smallest λ_{max} of 671 nm, which is 21 nm red-shifted compared to BF$_2$(ADP) (650 nm). This is consistent with the thiophenes acting as electron rich substituents that are not conjugated with the ADP core. Using phenylethynyl (**3**) or *p*-alkylphenylethynyl (**1**) substituents increased λ_{max} to 732 nm and 736 nm, respectively, consistent with conjugation between the phenylethynyl groups and the ADP core. Adding electron-donating groups in the pyrrolic substituents further increased λ_{max} to 757 nm and 758 nm for *p*-alkoxyphenylethynyl (**4**) and thienylethynyl (**5**) substituents, respectively. These λ_{max} values are significantly larger than those of the respective free ligands, with a change of: 111 nm for
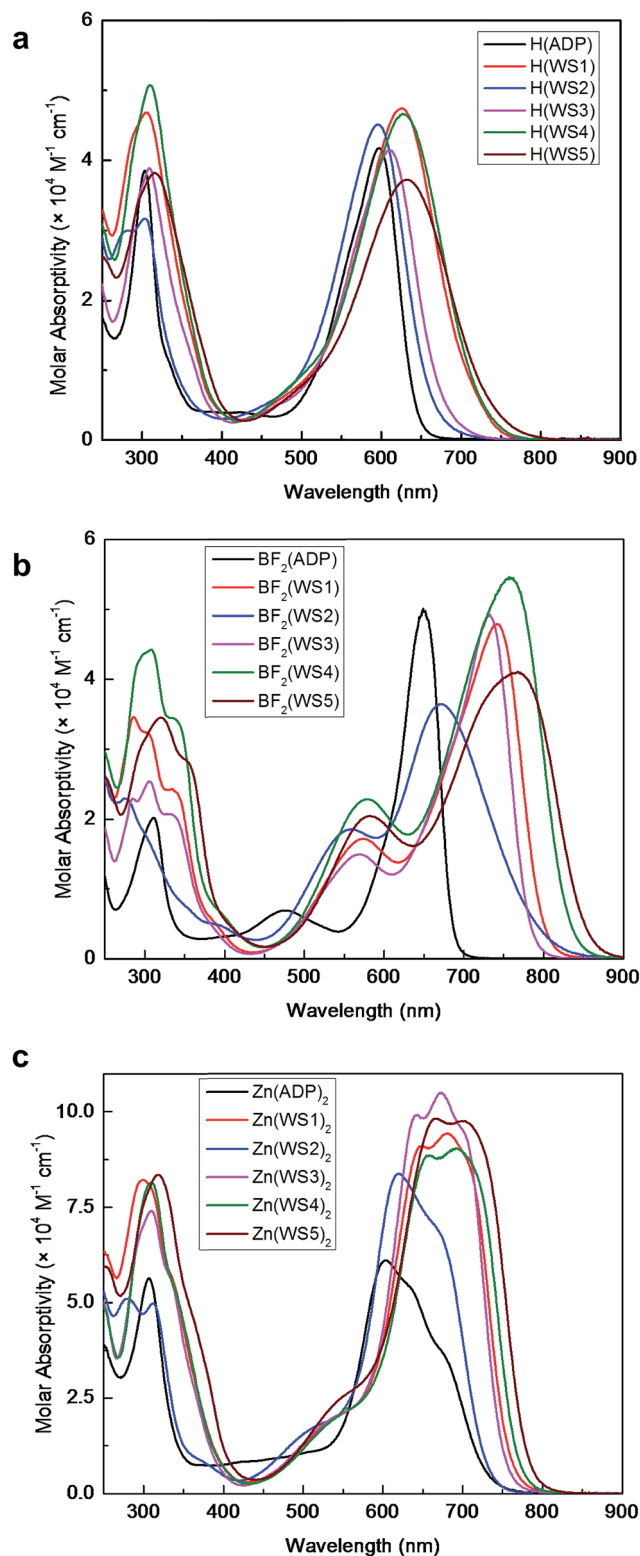

Fig. 4 Absorption spectra of (a) H(ADP) and H(WS1–5) (b) BF$_2$$^+$ chelates, and (c) Zn(ɪɪ) complexes in chloroform solutions.

BF$_2$(WS1), 77 nm for BF$_2$(WS2), 122 nm for BF$_2$(WS3), 128 nm for BF$_2$(WS4), and 135 nm for BF$_2$(WS5). These red-shifts are all larger than that observed for BF$_2$(ADP) (50 nm). These significant bathochromic shifts are attributed to the enforced

Table 2 Summary of optical properties of ADP-based molecules in solution and film

	Solution		Film	
	λ_{max}, nm (ε, $\times 10^3$ M^{-1} cm^{-1})	λ_{onset}, nm	$\lambda_{max}^{visible}$, nm	λ_{onset}, nm
H(ADP)	302 (38), 596 (42)	645	640	740
BF$_2$(ADP)	310 (20), 649 (50)	688	711	810
Zn(ADP)$_2$	302 (57), 591 (78), 645 (51)	713	650	735
H(WS1)	302 (46), 625 (47)	715	612	765
BF$_2$(WS1)	307 (32), 741 (48)	798	763	835
Zn(WS1)$_2$	300 (82), 650 (91), 683 (94)	764	707	780
H(WS2)	305 (45), 594 (32)	659	528	675
BF$_2$(WS2)	275 (23), 671 (36)	800	654	795
Zn(WS2)$_2$	278 (51), 620 (84), 676 (66)	737	622	745
H(WS3)	309 (39), 610 (42)	676	585	775
BF$_2$(WS3)	306 (25), 732 (49)	782	763	845
Zn(WS3)$_2$	309 (39), 674 (105), 705 (93)	757	696	785
H(WS4)	309 (51), 629 (47)	725	597	820
BF$_2$(WS4)	310 (44), 757 (55)	830	780	880
Zn(WS4)$_2$	310 (81), 655 (88), 693 (90)	780	709	785
H(WS5)	315 (38), 633 (37)	736	645	870
BF$_2$(WS5)	320 (34), 768 (41)	850	750	890
Zn(WS5)$_2$	318 (84), 665 (98), 702 (97)	780	722	815

planarity and extended conjugation through aryl groups. The BF$_2$$^+$ chelates in chloroform weakly emitted in the near-infrared (λ_{max} 794–853 nm, see ESI section†).

Fig. 4c shows the absorption spectra of the Zn(II) complexes. Generally, the Zn(II) complexes have a broad absorption in the visible to near-infrared region, with very high molar absorptivity ranging from 88×10^3 M^{-1} cm^{-1} to 98×10^3 M^{-1} cm^{-1}. The Zn(WS1, 3–5)$_2$ complexes exhibited two overlapping absorptions, resulting from a combination of ligand planarization upon Zn(II) chelation and exciton coupling of the two planar ligands.[43] All Zn(II) complexes were non-fluorescent.

To evaluate the optical properties in the film, we fabricated films on glass slides by spin-coating from chloroform solutions. The Zn(II) complex films were more uniform than those of the free ligands or BF$_2$$^+$ chelates. The films were bright blue for free ligands and BF$_2$$^+$ chelates, and blue-red for the Zn(II) complexes. The optical properties of the films are summarized in Table 2. The low energy absorption extended well into the near-infrared region. Depending on the pyrrolic substituents, onsets ranged from 675 nm to 870 nm for free ligands, 810 nm to 890 nm for BF$_2$$^+$ chelates and 735 nm to 815 nm for Zn^{2+} chelates. The absorption spectra of solution and film are compared in Fig. S15† and the shifts upon film formation are summarized in Table S3.† In general, the absorption spectra of films were broader than in solution and the absorption onset shifted to longer wavelengths upon film formation (with the exception of BF$_2$(WS2), which slightly blue-shifted upon film formation). On the other hand, the low energy absorption maximum either red-shifted or blue-shifted upon film formation, depending on the pyrrolic substituent and chelation used. This indicates that the pyrrolic substituents and chelation affect molecular packing in the solid state.

To evaluate how the absorption of our acceptors complement that of P3HT, we obtained the thin film absorption spectra of 1 : 1 w/w mixtures of ADP derivatives and P3HT. Fig. 5a shows UV-Vis absorption spectra of free ligands mixed with P3HT. The absorption of the mixture was similar to that of neat P3HT, partly because the absorption of the free ligands overlaps with that of P3HT. Nevertheless, there were a few differences: the λ_{max} for P3HT/H(WS2) was blue shifted compared to neat P3HT, while others have red-shifted absorption by ~10–30 nm. A significant absorption near ~300 nm, which is not present in neat P3HT, is attributed to the absorption from the ADP ligands. Fig. 5b depicts the absorption spectra of P3HT mixed with BF$_2$$^+$ chelates. Compared to neat P3HT, the blends had extra absorption bands near 300 nm and in the near-IR range ~650–900 nm, due to the absorption of the BF$_2$$^+$ chelates that nicely complement that of P3HT. Fig. 5c illustrates the film absorption spectra of the P3HT blend with Zn(II) complexes. The absorption spectra of the Zn(II) complexes also complement those of P3HT, extending the absorption of P3HT near 300 nm and in the ~650–800 nm for a better overlap with the solar spectrum.

One pre-requisite for good organic solar cells is efficient exciton dissociation, which can be probed using fluorescence quenching experiments. Fig. S17† compares the fluorescence of the neat P3HT film with that of blend films (spin-coated from 1 : 1 w/w mixtures). The data for ADP and WS1 series were previously published in a separate study and are included in Fig. S17† for comparison.[37] The films were excited at 360 nm. Although azadipyrromethene dyes can also be excited at 360 nm, free ligands and Zn(II) complexes do not fluoresce and BF$_2$$^+$ chelates have very weak emission at longer wavelengths than P3HT, and thus do not interfere with the fluorescence of P3HT. All free ligands and chelates quenched the fluorescence of P3HT, consistent with exciton dissociation. Quenching was not complete for the free ligands H(ADP), H(WS2), H(WS3) and H(WS4). Incomplete quenching could be due to either lower quenching ability or to a larger phase separation between P3HT and acceptor. Our previous work reported that H(ADP) and H(WS1) have similar Stern–Volmer quenching constants in solution (and both are slightly higher than that of PCBM). We therefore concluded that the lower quenching efficiency of H(ADP) than H(WS1) in blend films was caused by a larger phase separation scale (also observed by AFM).[37] Based on these results, it is reasonable to hypothesize that the incomplete quenching of the free ligands H(WS2), H(WS3) and H(WS4) are also caused by larger phase separation between the ligand and P3HT.

Photovoltaic properties

The photovoltaic properties of the azadipyrromethene-based dyes were studied in inverted organic solar cells using P3HT as the electron donor. The device configuration was ITO/ZnO/P3HT : Zn(WS1–5)$_2$ (90 nm)/MoO$_3$ (10 nm)/Ag (80 nm). In our hands, free ligands and BF$_2$$^+$ chelates did not give any significant photovoltaic effects, most likely due to unfavorable blend morphologies. On the other hand, the zinc(II) chelates all
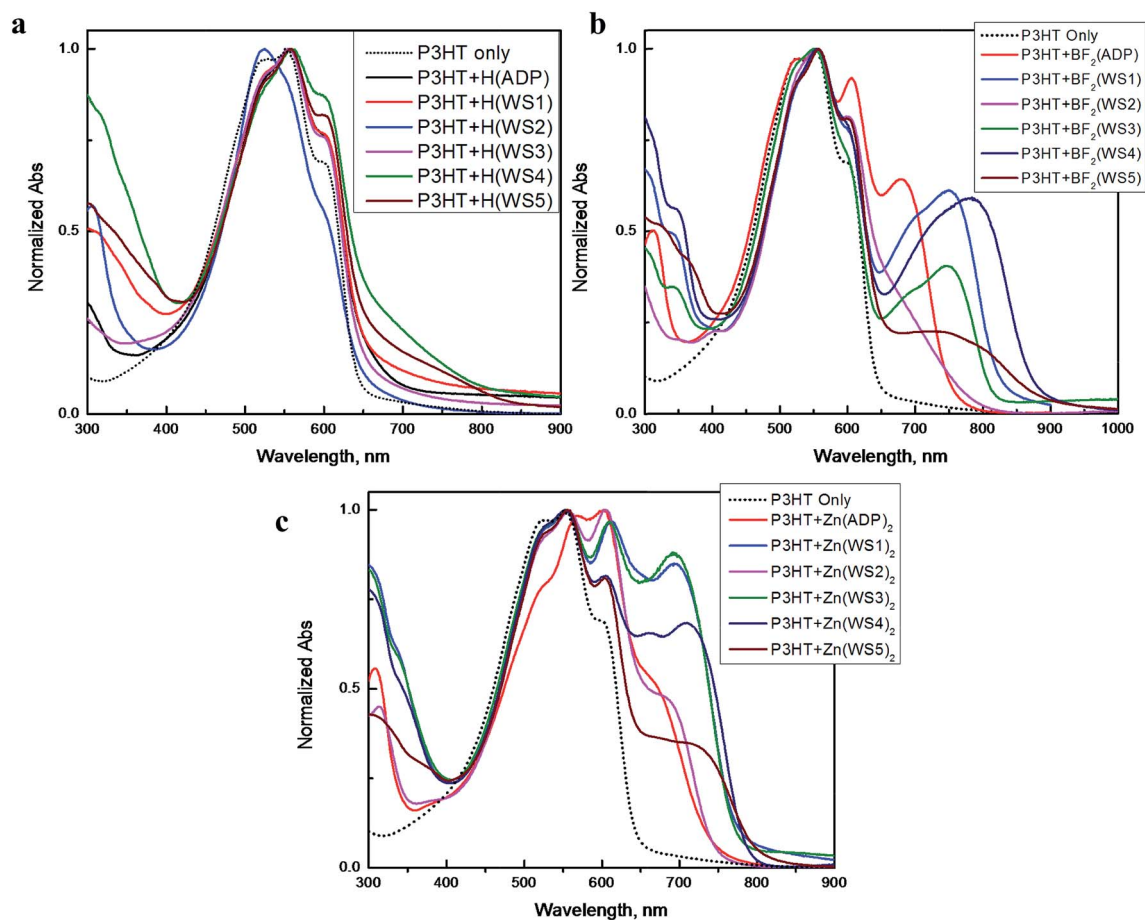
Fig. 5 Film absorption spectra of the P3HT blend with ADP-based materials.

showed good photovoltaic properties. We performed some device processing optimization, which involved a screening of total concentrations (film thickness), annealing conditions and blend weight ratios using *ortho*-dichlorobenzene as the solvent. We found that the best results were obtained with a total concentration of 20 mg mL^{-1} and annealing at 120 °C for 30 min prior to top electrode deposition. The optimal blend ratio (by weight) varied from 1 : 0.5 to 1 : 1 P3HT : acceptor.

Fig. 6 shows the current–voltage curves obtained for the best P3HT : Zn(WS1–5)$_2$ devices, and Table 3 summarizes the device parameters, including the parameters for the best devices and the parameter averages of 8 to 10 devices. All current–voltage curves show a diode behavior. The PCE obtained for the zinc acceptors varied between ∼2% and 4%. Interestingly, all had a higher PCE than Zn(ADP) with no pyrrolic substituents. This suggests that the pyrrolic substituents are beneficial for a higher PCE. Zn(WS2)$_2$ with thiophene pyrrolic substituents showed a PCE of 2.1%, a J_{sc} of 4.8 mA cm^{-2}, a V_{oc} of 0.9 V, and a FF of 49%. This acceptor had the largest V_{oc} due to its higher LUMO energy level. Adding an ethynyl spacer between the ADP core and thiophene increased the PCE to 2.7% (Zn(WS5)$_2$). Zn(WS4)$_2$ had a similar PCE of 2.6%, despite changing the aryl group to phenyl. Zn(WS1)$_2$ had a slightly higher PCE of 2.9%,

suggesting that the *t*-butyl groups are slightly better than 2-ethylhexyl. This is somewhat surprising, as *t*-butyl solubilizing groups are usually avoided in the design of conjugated materials, as they are thought to be bulky. The best cell was obtained from Zn(WS3)$_2$ with no alkyl groups, with a PCE of 4.1%.
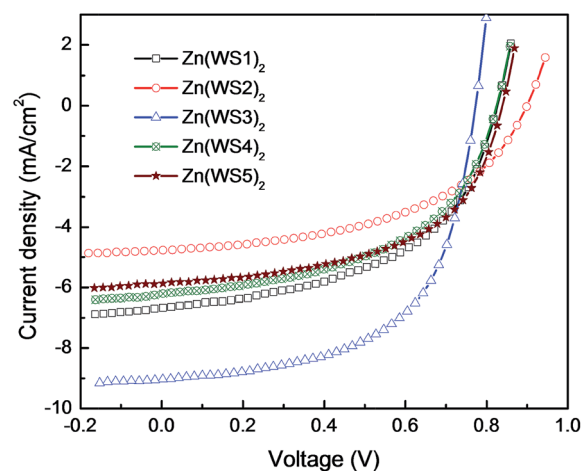

Fig. 6 Current–voltage curves for the best P3HT : Zn(WS1–5)$_2$ solar cells.

**Table 3** Photovoltaic performance of blends of P3HT with zinc complexes (20 mg mL^{-1}, annealed 120 °C, 30 min)

Donor : acceptor	Weight ratio	V_{oc} (V)	J_{sc} (mA cm^{-2})	FF (%)	PCE (%)
P3HT : ADP	1 : 0.7	0.82 (0.81 ± 0.01)	2.8 (3.0 ± 0.3)	60 (59 ± 1)	1.4 (1.3 ± 0.1)
P3HT : Zn(WS1)$_2$	1 : 0.5	0.83 (0.82 ± 0.01)	6.7 (6.5 ± 0.2)	52 (51 ± 2)	2.9 (2.7 ± 0.1)
P3HT : Zn(WS2)$_2$	1 : 1	0.91 (0.89 ± 0.02)	5.0 (4.5 ± 0.5)	49 (47 ± 3)	2.2 (1.9 ± 0.2)
P3HT : Zn(WS3)$_2$	1 : 0.7	0.77 (0.76 ± 0.01)	9.1 (8.8 ± 0.5)	59 (57 ± 3)	4.1 (3.9 ± 0.2)
P3HT : Zn(WS4)$_2$	1 : 0.5	0.82 (0.82 ± 0.45)	6.2 (5.7 ± 0.5)	51 (49 ± 2)	2.6 (2.3 ± 0.1)
P3HT : Zn(WS5)$_2$	1 : 0.7	0.84 (0.82 ± 0.02)	5.9 (5.9 ± 0.3)	55 (53 ± 0.1)	2.7 (2.6 ± 0.1)
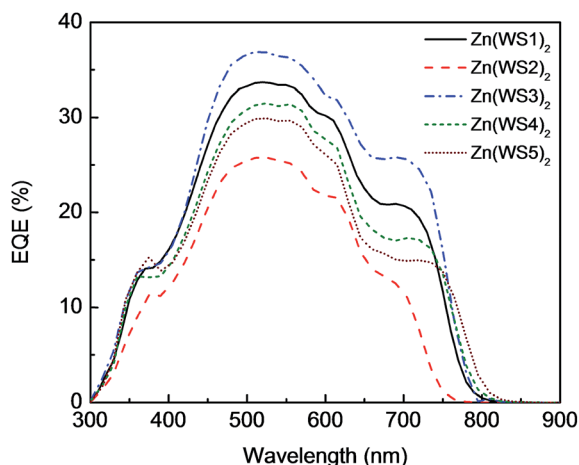
Fig. 7 External quantum yield spectra for the best P3HT : Zn(WS1–5)$_2$ solar cells.

It appears that the differences in the PCE between the acceptors is mainly governed by J_{sc}, which can be influenced by several factors including the absorption spectra, as well as charge separation and charge extraction efficiency. Fig. 7 depicts the incident photon-to-current efficiency (IPCE) spectra of the best solar cells. All P3HT : Zn(WS1–5)$_2$ cells show a photoresponse beyond the absorption onset of P3HT, up to 800 nm, indicating that excitons generated in the acceptors contribute to photocurrent production. The spectral response of

Zn(WS2)$_2$ extended to shorter wavelength than the others, ~750 nm, which partly explains its lower J_{sc} and PCE compared to other complexes. However, the absorption spectra alone cannot explain the trends in J_{sc} and PCE observed, because all films had a thickness of ~90 nm. The maximum IPCEs at 510 nm were 26%, 30%, 31%, 34%, and 37% for Zn(WS2)$_2$, Zn(WS5)$_2$, Zn(WS4)$_2$, Zn(WS1)$_2$, andZn(WS3)$_2$, respectively. The ascending order for maximum IPCE correlates with that of J_{sc} and PCE.

Because device performance strongly depends on the morphology, we looked at the surface morphology of the active layer by atomic force microscopy (AFM). Images were taken directly from the best photovoltaic devices and are shown in Fig. 8. All blends had a similar nanoscale surface morphology, with no large-scale aggregates. This is in contrast to P3HT : Zn(ADP)$_2$, where large aggregates of Zn(ADP)$_2$ could be clearly seen.[36] This suggests that all pyrrolic substituents studied (including thienyl) prevent the formation of large aggregates. The surface roughness (root-mean-square) was 10.0, 9.8, 13.0, 9.7 and 8.4 nm for blends with Zn(WS1)$_2$, Zn(WS2)$_2$, Zn(WS3)$_2$, Zn(WS4)$_2$ and Zn(WS5)$_2$, respectively. These values are all similar and are comparable to the reported surface roughness of efficient P3HT:PCBM active layers.[44] Based on the photovoltaic and AFM results, we hypothesize that all Zn(WS1–5)$_2$ acceptors phase separate on a similar scale with P3HT, and that differences in performance arise from differences in local donor–acceptor interfaces that would be affected by the solubilizing groups. Additional studies are required to test this hypothesis.
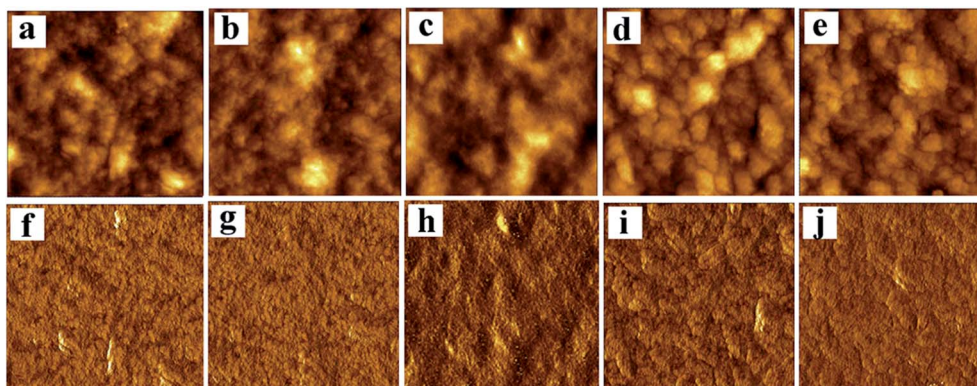
Fig. 8 Tapping-mode AFM height images (a–e) and phase images (f–j) for P3HT : acceptor blends taken directly from the active layers of the best cells reported in Table 3. The acceptor was: (a and f) Zn(WS1)$_2$; (b and g) Zn(WS2)$_2$; (c and h) Zn(WS3)$_2$; (d and i) Zn(WS4)$_2$; (e and j) Zn(WS5)$_2$. All images are 5 μm × 5 μm. The height scales were between 60 nm and 80 nm and the phase scale was between 30 and 40 degrees. Images with the scales are available in the ESI section.†

Conclusions

In this study, we explored the effects of pyrrolic substituents on the optical, electrochemical and photovoltaic properties of new electron acceptors based on azadipyrromethene complexes. The various modifications studied fine-tuned the optical and electrochemical properties of the ligands and complexes. In solar cells, the modifications of the zinc complexes did not dramatically affect the device performance and blend morphology. This shows the robustness of these acceptors when blended with P3HT as the donor. We made progress in identifying some of the design principles for electron accepting materials based on azadipyrromethene dyes. For example, comparing the performance of $Zn(WS3)_2$, $Zn(WS1)_2$ and $Zn(WS4)_4$ suggests that no solubilizing groups is better than t-butyl solubilizing groups, which is slightly better than 2-ethylhexyl solubilizing groups. Other less bulky solubilizing groups should be studied in the future to optimize solubility and performance. In addition, comparing the performance of $Zn(WS5)_2$ and $Zn(WS2)_2$ points to the importance of an ethynyl group between the azadipyrromethene core and the aryl group. We are currently exploring the effect of using a vinyl instead of an ethynyl group. Preliminary results with other high efficiency polymer donors (optimized for PCBM and $PC_{70}BM$ acceptors) have yielded poor results. The polymer donors tested had deeper HOMO and LUMO energy levels than P3HT, resulting in unfavorable energy matches with our acceptors. We are currently tuning the energy levels of $Zn(WS3)_2$ to test this hypothesis, continuing to learn how to design better non-fullerene acceptors for the next generation of organic photovoltaic devices.

Acknowledgements

References

1 C. Brabec, S. Gowrisanker, J. Halls, D. Laird, S. Jia and S. Williams, *Adv. Mater.*, 2010, **22**, 3839–3856.

2 *Organic Photovoltaics: Materials, Device Physics, and Manufacturing Technologies*, ed. C. Brabec, V. Dyakonov and U. Scherf, WILEY-VCH Verlag GmbH & Co. KGaA, Weinheim, 2008.

3 F. C. Krebs, S. A. Gevorgyan and J. Alstrup, *J. Mater. Chem.*, 2009, **19**, 5442–5451.

4 N. Espinosa, M. Hösel, M. Jørgensen and F. C. Krebs, *Energy Environ. Sci.*, 2014, **7**, 855–866.

5 J. Nelson, *Mater. Today*, 2011, **14**, 462–470.

6 L. Dou, J. You, Z. Hong, Z. Xu, G. Li, R. A. Street and Y. Yang, *Adv. Mater.*, 2013, **25**, 6642–6671.

7 Y. He and Y. Li, *Phys. Chem. Chem. Phys.*, 2011, **13**, 1970–1983.

8 A. M. Nardes, A. J. Ferguson, P. Wolfer, K. Gui, P. L. Burn, P. Meredith and N. Kopidakis, *ChemPhysChem*, 2014, **15**, 1539–1549.

9 R. D. Pensack, C. Guo, K. Vakhshouri, E. D. Gomez and J. B. Asbury, *J. Phys. Chem. C*, 2012, **116**, 4824–4831.

10 J. Peet, M. L. Senatore, A. J. Heeger and G. C. Bazan, *Adv. Mater.*, 2009, **21**, 1521–1527.

11 A. Facchetti, *Mater. Today*, 2013, **16**, 123–132.

12 K. Cnops, B. P. Rand, D. Cheyns, B. Verreet, M. A. Empl and P. Heremans, *Nat. Commun.*, 2014, **5**, 3406.

13 Y. Zang, C.-Z. Li, C.-C. Chueh, S. T. Williams, W. Jiang, Z.-H. Wang, J.-S. Yu and A. K. Y. Jen, *Adv. Mater.*, 2014, **26**, 5708–5714.

14 Y. Zhou, T. Kurosawa, W. Ma, Y. Guo, L. Fang, K. Vandewal, Y. Diao, C. Wang, Q. Yan, J. Reinspach, J. Mei, A. L. Appleton, G. I. Koleilat, Y. Gao, S. C. B. Mannsfeld, A. Salleo, H. Ade, D. Zhao and Z. Bao, *Adv. Mater.*, 2014, **26**, 3767–3772.

15 Z. Lu, B. Jiang, X. Zhang, A. Tang, L. Chen, C. Zhan and J. Yao, *Chem. Mater.*, 2014, **26**, 2907–2914.

16 W. Jiang, L. Ye, X. Li, C. Xiao, F. Tan, W. Zhao, J. Hou and Z. Wang, *Chem. Commun.*, 2014, **50**, 1024–1026.

17 T. Earmme, Y. J. Hwang, N. M. Murari, S. Subramaniyan and S. A. Jenekhe, *J. Am. Chem. Soc.*, 2013, **135**, 14960–14963.

18 J. T. Bloking, T. Giovenzana, A. T. Higgs, A. J. Ponec, E. T. Hoke, K. Vandewal, S. Ko, Z. Bao, A. Sellinger and M. D. McGehee, *Adv. Energy Mater.*, 2014, **4**, 1301426.

19 B. Verreet, K. Cnops, D. Cheyns, P. Heremans, A. Stesmans, G. Zango, C. G. Claessens, T. Torres and B. P. Rand, *Adv. Energy Mater.*, 2014, **4**, 1301413.

20 X. Zhang, Z. Lu, L. Ye, C. Zhan, J. Hou, S. Zhang, B. Jiang, Y. Zhao, J. Huang, S. Zhang, Y. Liu, Q. Shi, Y. Liu and J. Yao, *Adv. Mater.*, 2013, **25**, 5791–5797.

21 P. Cheng, L. Ye, X. Zhao, J. Hou, Y. Li and X. Zhan, *Energy Environ. Sci.*, 2014, **7**, 1351–1356.

22 Y. Zhou, Y.-Z. Dai, Y.-Q. Zheng, X.-Y. Wang, J.-Y. Wang and J. Pei, *Chem. Commun.*, 2013, **49**, 5802–5804.

23 Y. Lin, Y. Wang, J. Wang, J. Hou, Y. Li, D. Zhu and X. Zhan, *Adv. Mater.*, 2014, **26**, 5137–5142.

24 A. a. F. Eftaiha, J.-P. Sun, I. G. Hill and G. C. Welch, *J. Mater. Chem. A*, 2014, **2**, 1201–1213.

25 Y. Kim and E. Lim, *Polymers*, 2014, **6**, 382–407.

26 J. E. Anthony, A. Facchetti, M. Heeney, S. R. Marder and X. Zhan, *Adv. Mater.*, 2010, **22**, 3876–3892.

27 P. Hudhomme, *EPJ Photovoltaics*, 2013, **4**, 40401–40411.

28 J. E. Anthony, *Chem. Mater.*, 2011, **23**, 583–590.

29 P. Sonar, J. P. Fong Lim and K. L. Chan, *Energy Environ. Sci.*, 2011, **4**, 1558–1574.

30 A. Loudet and K. Burgess, *Chem. Rev.*, 2007, **107**, 4891–4932.

31 D. V. Partyka, N. Deligonul, M. P. Washington and T. G. Gray, *Organometallics*, 2009, **28**, 5837–5840.

32 A. Palma, J. F. Gallagher, H. Mueller-Bunz, J. Wolowska, E. J. L. McInnes and D. F. O'Shea, *Dalton Trans.*, 2009, 273–279.

33 A. Gorman, J. Killoran, C. O'Shea, T. Kenna, W. M. Gallagher and D. F. O'Shea, *J. Am. Chem. Soc.*, 2004, **126**, 10619–10631.

34 V. Bandi, K. Ohkubo, S. Fukuzumi and F. D'Souza, *Chem. Commun.*, 2013, **49**, 2867–2869.

35 A. M. Poe, A. M. Della Pelle, A. V. Subrahmanyam, W. White, G. Wantz and S. Thayumanavan, *Chem. Commun.*, 2014, **50**, 2913–2915.

36 Z. Mao, W. Senevirathna, J. Y. Liao, J. Gu, S. V. Kesava, C. Guo, E. D. Gomez and G. Sauve, *Adv. Mater.*, 2014, **26**, 6290–6294.

37 W. Senevirathna and G. Sauve, *J. Mater. Chem. C*, 2013, **1**, 6684–6694.

38 S. Rajaram, R. Shivanna, S. K. Kandappa and K. S. Narayan, *J. Phys. Chem. Lett.*, 2012, **3**, 2405–2408.

39 Q. Yan, Y. Zhou, Y.-Q. Zheng, J. Pei and D. Zhao, *Chem. Sci.*, 2013, **4**, 4389–4394.

40 C. Xia, X. Fan, J. Locklin and R. C. Advincula, *Org. Lett.*, 2002, **4**, 2067–2070.

41 R. Gresser, H. Hartmann, M. Wrackmeyer, K. Leo and M. Riede, *Tetrahedron*, 2011, **67**, 7148–7155.

42 C. M. Cardona, W. Li, A. E. Kaifer, D. Stockdale and G. C. Bazan, *Adv. Mater.*, 2011, **23**, 2367–2371.

43 S. G. Telfer, T. M. McLean and M. R. Waterland, *Dalton Trans.*, 2011, **40**, 3097–3108.

44 G. Li, V. Shrotriya, J. Huang, Y. Yao, T. Moriarty, K. Emery and Y. Yang, *Nat. Mater.*, 2005, **4**, 864–868.